Journal of Non-Newtonian Fluid Mechanics 248 (2017) 8–22

Contents lists available at ScienceDirect

Journal of Non-Newtonian Fluid Mechanics

journal homepage: www.elsevier.com/locate/jnnfm

Viscoplastic flow development in a channel with slip along one wall

Pandelitsa Panaseti, Georgios C. Georgiou*

Department of Mathematics and Statistics, University of Cyprus, PO Box 20537, 1678 Nicosia, Cyprus

ARTICLE INFO

Article history:
Received 3 June 2017
Revised 9 August 2017
Accepted 27 August 2017
Available online 30 August 2017

Keywords:
Plane Poiseuille Flow
Bingham plastic
Wall slip
Navier slip
Flow development
Development length
Finite elements

ABSTRACT

The flow development of a Herschel–Bulkley fluid in a horizontal channel is considered assuming that slip occurs only on the upper wall due to slip heterogeneities. Hence, the velocity profile is allowed to be asymmetric as was the case in recent experiments on softy glassy suspensions [13]. A power-law slip equation is employed, which generalizes the Navier-slip law. The one-dimensional fully-developed solutions are derived and the different flow regimes are identified. The two-dimensional development flow is solved numerically using finite elements along with the Papanastasiou regularization for the constitutive equation. Due to the asymmetry and the viscoplastic character of the flow, the classical definition of the development length is not applicable. The global and upper-wall development lengths are thus considered and the combined effects of slip and the Bingham number are investigated. Numerical results are presented for two values of the power-law exponent, i.e. $n=1$ (Bingham plastic) and $n=1/2$ (Herchel–Bulkley fluid). It is demonstrated that the global development length increases with the Bingham number and that flow development is slower near the no-slip wall. The global development length increases with slip exhibiting two plateaus and an intermediate rapid increase zone and doubles in the limit of infinite slip.

1. Introduction

Many materials of industrial interest, such as polymeric solutions, suspensions, and gels, are viscoplastic, i.e. they exhibit yield stress. These materials behave as fluids when the exerted stress exceeds the yield stress and as solids otherwise. A popular viscoplastic constitutive equation which also describes shear-thinning or shear thickening is the Herschel–Bulkley model, which involves three material parameters, i.e. the yield stress τ_0, the consistency index k, and the power-law exponent, n [1]. The tensorial form of this model is as follows:

$$\begin{cases} \dot{\boldsymbol{\gamma}} = \mathbf{0}, & \tau \le \tau_0 \\ \boldsymbol{\tau} = \left(\dfrac{\tau_0}{\dot{\gamma}} + k\dot{\gamma}^{n-1} \right) \dot{\boldsymbol{\gamma}}, & \tau > \tau_0 \end{cases} \tag{1}$$

where $\boldsymbol{\tau}$ is the viscous stress tensor, $\dot{\boldsymbol{\gamma}} \equiv \nabla\mathbf{u} + (\nabla\mathbf{u})^T$ is the rate of strain tensor, $\mathbf{u}$ is the velocity vector, $\nabla\mathbf{u}$ is the velocity gradient tensor, and the superscript T denotes its transpose. The magnitudes of $\dot{\boldsymbol{\gamma}}$ and $\boldsymbol{\tau}$, denoted respectively by $\dot{\gamma}$ and τ, are defined by $\dot{\gamma} \equiv \sqrt{\dot{\boldsymbol{\gamma}} : \dot{\boldsymbol{\gamma}}/2}$ and $\tau \equiv \sqrt{\boldsymbol{\tau} : \boldsymbol{\tau}/2}$. The Herschel–Bulkley model is reduced to the power-law model when the yield stress is zero and to the Bingham-plastic model when $n=1$.

In flows of ideal yield-stress fluids, the flow domain consists of the so-called unyielded ($\tau \le \tau_0$) and yielded regions ($\tau > \tau_0$) where the two branches of the constitutive equation apply. The former regions include zones where the material moves undeformed as a rigid body and dead zones where it is stagnant. Determining the interfaces between yielded and unyielded regions is a key computational challenge with viscoplastic fluid flows, especially in two- and three-dimensional flows [2]. Two are the main approaches to tackle this problem: (a) Augmented Lagrangian Methods (ALMs); and (b) Regularization methods. ALMs are based on the variational formulation of the Navier–Stokes equations and employ optimization algorithms to determine the flow solution [2]. They are exact in the sense that they respect the discontinuous form of the constitutive equation. However, ALMs are generally slower and more difficult to implement than regularization methods [2].

In regularization methods, the constitutive equation is modified by introducing an additional parameter in order to combine the two branches of Eq. (1) into one smooth function, so that the resulting regularized equation applies everywhere in the flow field in both yielded and (practically) unyielded regions. The most popular regularization in the literature is that proposed by Papanastasiou [3] for a Bingham plastic and subsequently by Ellwood et al. [4] for a Herschel–Bulkley fluid:

$$\boldsymbol{\tau} = \left\{ \frac{\tau_0[1 - \exp(-m\dot{\gamma})]}{\dot{\gamma}} + k\dot{\gamma}^{n-1} \right\} \dot{\boldsymbol{\gamma}} \tag{2}$$

* Corresponding author.
E-mail address: georgios@ucy.ac.cy (G.C. Georgiou).

http://dx.doi.org/10.1016/j.jnnfm.2017.08.008
0377-0257/

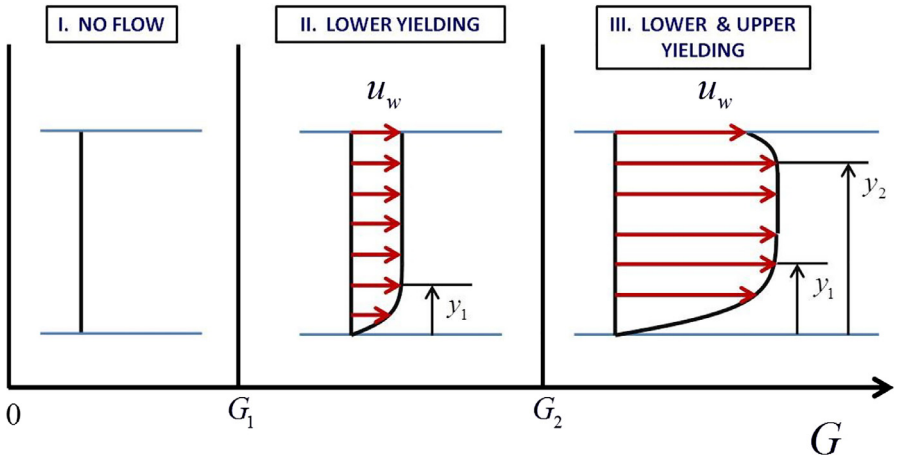

Fig. 1. Different flow regimes in the case of one-dimensional plane viscoplastic Poiseuille flow when slip occurs only along the upper wall.

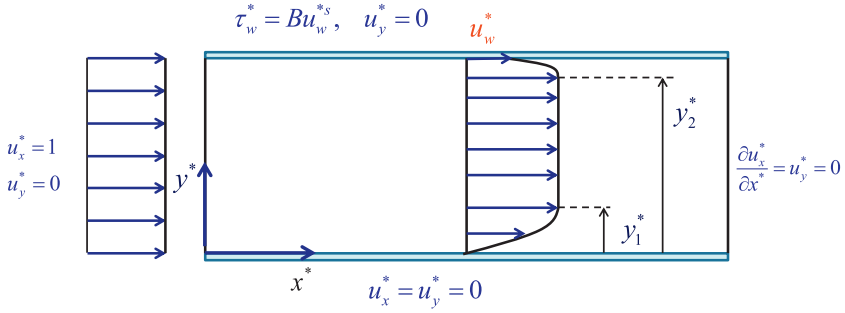

Fig. 2. Geometry and boundary conditions of the flow development of a Bingham plastic in a horizontal channel with slip along the upper wall.

where m is the stress growth exponent, which has dimensions of time. For sufficiently large values of m the Papanastasiou model provides a satisfactory approximation of the Bingham-plastic model. The regularized approach is easier to implement than ALMs but eliminates the yield surfaces replacing unyielded regions with regions of very high viscosity. The interface of yielded/"unyielded" regions can approximately be tracked down a posteriori by using the von Mises criterion $\boldsymbol{\tau} = \boldsymbol{\tau}_0$ [1,5]. The advantages and disadvantages of ALMs and regularization methods are discussed in the recent articles of Balmforth et al. [2] and Saramito and Wachs [6].

Wall slip is important in many industrial applications, such as the extrusion of complex fluids, ink jet processes, oil migration in porous media, and in microfluidics. Viscoplastic materials are known to exhibit wall slip [7–9]. While wall slip with polymer melts is observed at large rates of strains, with pasty materials it appears within a range of rather small strains [10]. Based on the analysis of apparent slip flows of Herschel–Bulkley fluids in various geometries, Kalyon [11] proposed a power-law slip equation, relating the wall shear stress, $\boldsymbol{\tau}_w$, to the slip (or sliding) velocity, u_w, defined as the relative velocity of the fluid with respect to that of the wall,

$$\boldsymbol{\tau}_w = \beta u_w^s \tag{3}$$

where s is the exponent, and β is the slip coefficient. The latter coefficient incorporates the effects of temperature, the normal stress, the molecular parameters, and the properties of the fluid/wall interface [10]. The no-slip and full-slip limiting cases are recovered when $\beta \to \infty$ and $\beta = 0$, respectively. Experimental values of the exponent s have been reviewed by Panaseti et al. [14]. The value $s = 1$ has been reported in different experimental studies for stresses above the yield stress (see [14] and references therein). Setting $s = 1$ in Eq. (3) leads to the classical Navier-slip condition [12]

$$\boldsymbol{\tau}_w = \beta u_w \tag{4}$$

in which case the slip coefficient is related to the slip length b, by means of $\beta \equiv \mu/b$, where μ denotes the viscosity.

The present work is motivated by the recent findings of Vayssade et al. [13], who imaged the motion of well characterized softy glassy suspensions in microchannels whose walls impose different slip velocities. Their experiments showed that as the channel height decreases the flow ceases to be symmetric and slip heterogeneities effects become important. Interestingly, some of the experimental velocity profiles reported by Vayssade et al. are characterized by overshoots similar to those encountered in entry flows [13]. We thus revisit here the classical flow development problem of a Bingham plastic in a horizontal channel assuming, however, that power-law slip occurs along the upper wall only. The one-dimensional fully-developed flow with asymmetric slip along the two walls has been analyzed by Panaseti et al. [14]. The theoretical results compare well with the (fully-developed) experimental data of Vayssade et al. [13].

For the sake of simplicity, the special case where there is no slip along the lower wall is studied here. As illustrated in Fig. 1, three regimes are observed for the one-dimensional steady-state Poiseuille flow, as the pressure gradient G is increased. Below a certain critical value G_1 (Regime I) the lower wall shear stress is below the yield stress and thus there is no flow. In Regime II above G_1 and below a second critical pressure gradient G_2, the fluid yields only near the lower plate and the fluid adjacent to the upper wall slides as an unyielded plug. Finally, above G_2 at which the upper-wall shear stress also exceeds $\boldsymbol{\tau}_0$ (Regime III), the fluid yields near both the walls and the velocity profile is asymmetric with a plug core. In the special case when there is no slip along

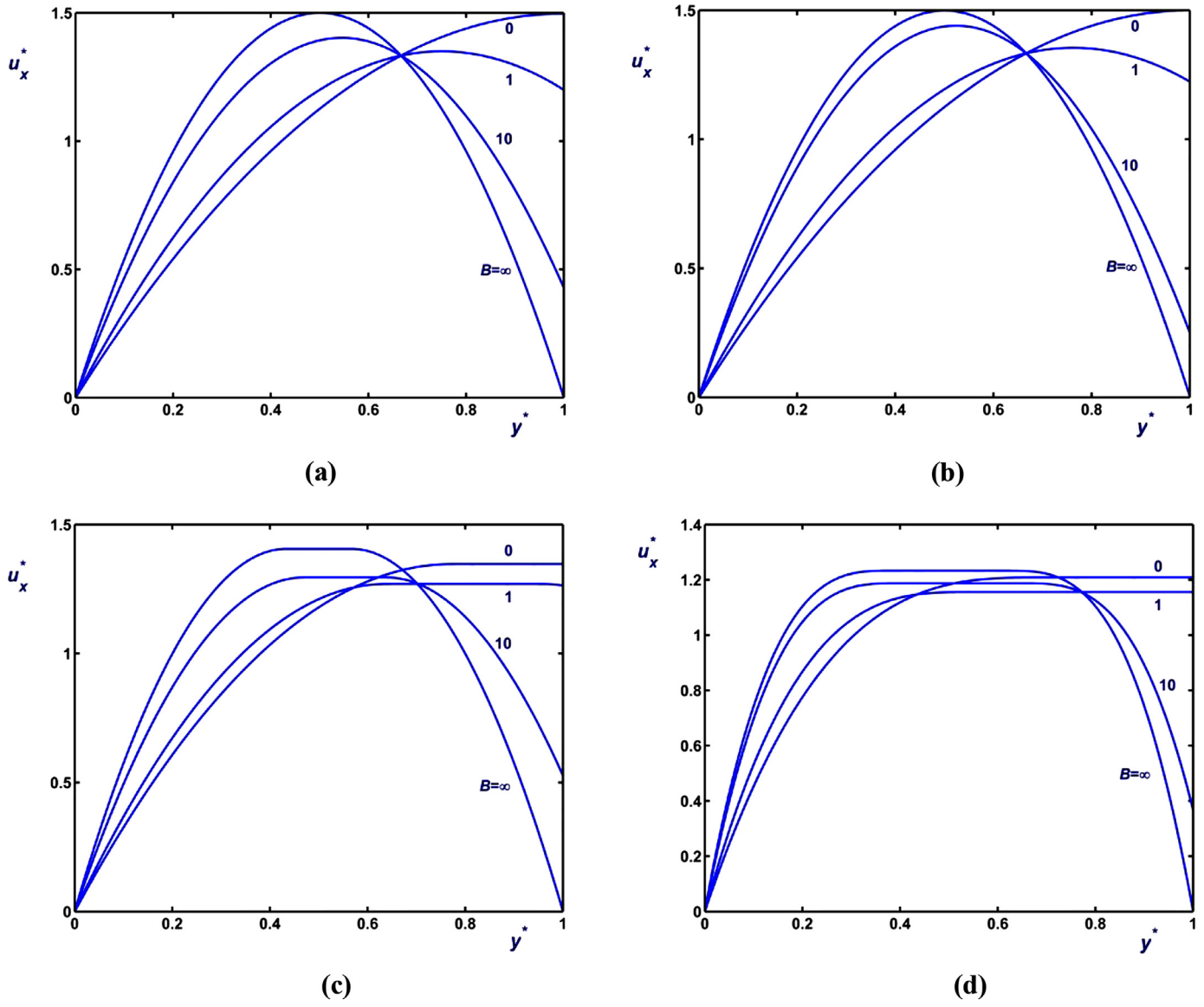

Fig. 3. Fully-developed velocity profiles for different values of the slip number in plane Poiseuille flow with no-slip along the lower wall and slip along the upper one: (a) $Bn=0$ (Newtonian flow) and $s=1$ (Navier slip); (b) $Bn=0$ (Newtonian flow) and $s=1/2$; (c) $Bn=1$, $n=1$ (Bingham flow) and $s=1$ (Navier slip); (d) $Bn=1$, $n=1/2$ (Herschel–Bulkley flow) and $s=1$ (Navier slip).

the upper wall, the classical symmetric Poiseuille solution is recovered and Regime II is not relevant.

The flow development problem is obviously two-dimensional: the fluid enters a tube or a channel at a uniform velocity and decelerates near the wall(s) and accelerates in the central region. In other words, the axial velocity tends from a flat profile at the inlet to the fully-developed profile downstream. The development length is usually defined as the length required for the maximum velocity to attain 99% of its fully-developed value scaled either by the pipe diameter or the channel width [15]. This definition implies that the maximum velocity in the central acceleration region develops more slowly than its counterparts at any other vertical distance from the axis or plane of symmetry. This may not be the case in all geometries and for all fluids, especially viscoplastic ones which are characterized by a maximum flat velocity. It is also clear that such a definition is not applicable in the case of asymmetric Poiseuille flow which is of interest here. In a recent study of the effect of wall slip on the development of planar and axisymmetric Newtonian Poiseuille flows, Kountouriotis et al. [16] pointed out that in addition to the standard definition of the development length, L, as the length required for the maximum velocity to attain 99% of its fully-developed value, the wall development length L_w is also relevant in the presence of slip. This is defined as the length required for the slip velocity to decrease to 1.01% of its fully-developed value. The numerical simulations of Kountouriotis et al. [16] showed that both L and L_w increase with slip passing through a maximum and vanish at a critical value of the slip parameter corresponding to the full slip case. They also revealed that, in contrast to the axisymmetric flow, the planar flow develops more slowly at the wall than at the midplane, i.e. $L_w > L$.

In a subsequent work, Philippou et al. [17] studied numerically the development of Bingham plastic flow in tubes and channels using the Papanastasiou regularization and finite element simulations. They considered alternative definitions of the development length noting that this is a function of the transversal coordinate. Their results demonstrated that the classical development length, L_c, and the development length, L_{95}, proposed by Ookawara et al. [18] for Bingham flow are not good choices for measuring vis-

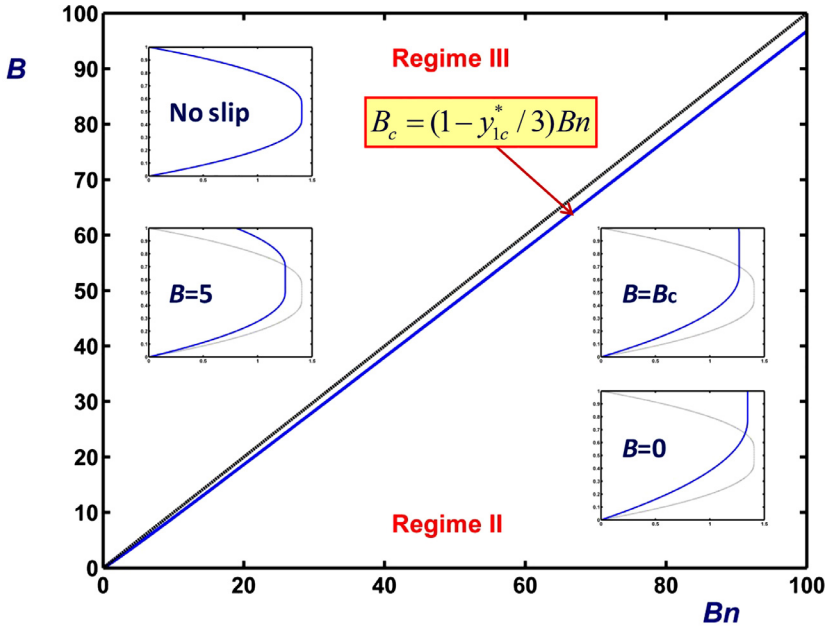

Fig. 4. Flow regimes and representative velocity profiles in plane Bingham-plastic flow with no-slip along the lower wall and Navier slip ($s = 1$) along the upper one. The velocity profiles have been obtained for $Bn = 1$ and various slip numbers.

coplastic flow development (with or without slip). L_{95} is defined as the axial distance required for the velocity to reach 99% of the calculated maximum value at a radial location corresponding to 95% of the plug radius [18]. To avoid the inconsistencies resulting from the use of L_c and L_{95}, Philippou et al. [17] employed the global development length which in the case of a channel of width H is defined as follows

$$L_g \equiv \max_{0 \le y \le H} L(y) \tag{5}$$

$L(y)$ is the (smallest) length required for the two-dimensional axial velocity $u(x, y)$ to become equal to $0.99\,\bar{u}(y)$ or $1.01\,\bar{u}(y)$ when $\bar{u}(y) > \bar{u}_m$or $\bar{u}(y) < \bar{u}_m$, respectively, where $\bar{u}(y)$ is the fully-developed velocity profile and $\bar{u}_m$ is the mean velocity.

The present work can be viewed as an extension of [17] to the case of viscoplastic flow in a channel with slip only along one wall (asymmetric flow). The governing equations are presented in Section 2, where the analytical solutions corresponding to fully-developed flow for the case of a power-law slip equation are also derived and the various flow regimes are identified. In Section 3, the numerical method is briefly presented and the numerical results are discussed. Finally, the conclusions are summarized in Section 4.

2. Governing equations

The governing equations are de-dimensionalized scaling lengths by the gap height H of the channel, the velocity vector by the uniform inlet velocity U, and the pressure and the stress tensor components by kU^n/H^n. By denoting the de-dimensionalized variables with stars, the continuity and momentum equations for steady, incompressible flow with zero gravity can be written as follows:

$$\nabla^* \cdot \mathbf{u}^* = 0 \tag{6}$$

and

$$Re\,\mathbf{u}^* \cdot \nabla^* \mathbf{u}^* = -\nabla^* p^* + \nabla^* \cdot \boldsymbol{\tau}^* \tag{7}$$

where

$$Re \equiv \frac{\rho U^{2-n} H^n}{k} \tag{8}$$

is the Reynolds number, ρ being the constant density of the material.

The Pananastasiou regularization [3] is employed here for the Herschel–Bulkley model. The dimensionless form of the regularized constitutive equation may be written as follows:

$$\boldsymbol{\tau}^* = \left[Bn \frac{1 - \exp\left(-M\dot{\boldsymbol{\gamma}}^*\right)}{\dot{\boldsymbol{\gamma}}^*} + \dot{\boldsymbol{\gamma}}^{*n-1} \right] \dot{\boldsymbol{\gamma}}^* \tag{9}$$

where

$$Bn \equiv \frac{\tau_0 H^n}{kU^n} \tag{10}$$

is the Bingham number and

$$M \equiv \frac{mU}{H} \tag{11}$$

is the dimensionless growth exponent, which has to be sufficiently high so that the flow of the ideal discontinuous Herschel–Bulkley fluid is approximated satisfactorily [3–5].

The geometry and the boundary conditions of the flow are illustrated in Fig. 2. At the inlet plane, the velocity component in the direction of the flow is uniform ($u^*_x = 1$) and the transversal one vanishes. At the lower wall, there is no slip and no penetration and thus both velocity components are zero. At the upper wall the vertical velocity is again zero and slip is assumed to occur following a power-law slip equation,

$$\boldsymbol{\tau}^*_w = B u^{*s}_w \tag{12}$$

where

$$B \equiv \frac{\beta H^n}{kU^{n-s}} \tag{13}$$

is the (dimensionless) slip number. Note that B is the inverse of the slip number defined by Panaseti et al. [14]. Finally, the exit plane is taken sufficiently far downstream so that the flow can be assumed fully developed.

2.1. Fully-developed solutions

The de-dimensionalization introduced above is based on the mean velocity, which implies that there is flow, i.e. Regime I of

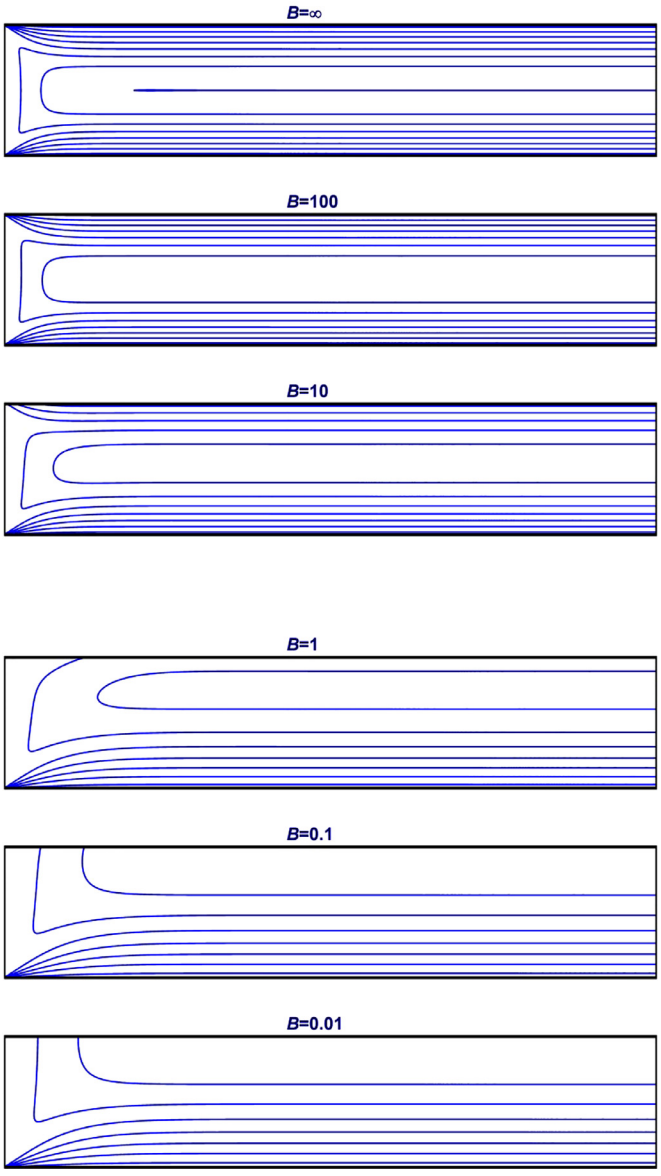

Fig. 5. Velocity contours in flow development of creeping ($Re=0$) planar Newtonian Poiseuille flow with no-slip along the lower wall and Navier slip ($s=1$) along the upper one for various slip numbers.

Fig. 1 is not relevant. The no-slip case, which corresponds to a symmetric velocity profile with respect to the mid-plane of the channel, is recovered for $B\to\infty$. The two yield points, y_1^* and y_2^*, are thus symmetric, i.e. $y_2^*=1-y_1^*$, and the flow is in Regime III (there is no Regime II). Keeping the Bingham number constant and decreasing the slip number, enhances slip at the upper wall and the velocity becomes asymmetric: the two yield points move towards the upper wall so that the width of the plug core $(y_2^*-y_1^*)$ increases while its velocity is reduced. This trend continues up to a critical slip number, B_c, at which the upper yield point reaches the wall (the dimensionless upper wall shear stress is equal to Bn) signaling the transition from Regime III to Regime II. Deriving the analytical solution is straightforward [14]. However, this is presented here for convenience and in order to account for the present scalings used and to identify the different flow regimes. The general dimensionless solution for $B_c\le B<\infty$ is given by

$$u_x^*(y^*)=\begin{cases}\dfrac{1}{A_{III}}\left[y_1^{*1/n+1}-(y_1^*-y^*)^{1/n+1}\right], & 0\le y^*\le y_1^*\\ \dfrac{y_1^{*1/n+1}}{A_{III}}, & y_1^*\le y^*\le y_2^*\\ u_w^*+\dfrac{1}{A_{III}}\left[(1-y_2^*)^{1/n+1}-(y^*-y_2^*)^{1/n+1}\right], & y_2^*\le y^*\le 1\end{cases} \tag{14}$$

where

$$u_w^*=\frac{1}{A_{III}}\left[y_1^{*1/n+1}-(1-y_2^*)^{1/n+1}\right] \tag{15}$$

and

$$A_{III}=y_1^{*1/n+1}\left(1-\frac{2n}{1+2n}y_1^*\right)-\frac{n}{1+2n}(1-y_2^*)^{1/n+2} \tag{16}$$

The positions of the two yield points can be found by solving the following system of equations:

$$(2-y_1^*-y_2^*)Bn-(y_2^*-y_1^*)Bu_w^{*s}=0 \tag{17}$$

and

$$(1+1/n)^n(y_2^*-y_1^*)-2Bn\,A_{III}^n=0 \tag{18}$$

2.1.1. No-slip case

In the no-slip case ($u_w^*=0$), Eq. (15) yields $y_2^*=1-y_1^*$, which indicates that the flow is symmetric with respect to the mid-plane of the channel. Substituting into Eq. (16) gives

$$A_{III}=y_1^{*1/n+1}\left(1-\frac{2n}{1+2n}y_1^*\right) \tag{19}$$

and Eq. (18) becomes:

$$(1+1/n)^n(1-2y_1^*)-2Bn\,y_1^{*n+1}\left(1-\frac{2n}{1+2n}y_1^*\right)^n=0 \tag{20}$$

2.1.2. Critical value of the slip number

The critical value B_c of the slip number can be found by setting $y_2^*=1$. Denoting the corresponding critical values of y_1^* and u_w^* by y_{1c}^* and u_{wc}^*, respectively, we get from Eq. (17)

$$B_c u_{wc}^{*s}=Bn \tag{21}$$

which simply says that the (dimensionless) upper-wall shear stress is equal to Bn. The critical slip velocity is given by

$$u_{wc}^*=\frac{1}{1-\frac{n}{1+2n}y_{1c}^*} \tag{22}$$

and, therefore,

$$B_c=\left(1-\frac{n}{1+2n}y_{1c}^*\right)^s Bn \tag{23}$$

Finally, from Eq. (18) one gets

$$(1+1/n)^n(1-y_{1c}^*)-2Bn\,A_{IIIc}^n=0 \tag{24}$$

or

$$(1+1/n)^n(1-y_{1c}^*)-2Bn\,y_{1c}^{*n+1}/u_{wc}^{*n}=0 \tag{25}$$

which is used to calculate y_{1c}^*. It should be noted that the value of y_{1c}^* is independent of the slip equation parameters. For example, in the Bingham plastic case ($n=1$), y_{1c}^* is a root of

$$Bn\,y_{1c}^{*3}-3Bn\,y_{1c}^{*2}-3y_{1c}^*+3=0 \tag{26}$$

while the value of B_c can then be calculated from Eq. (23) for any value of s.

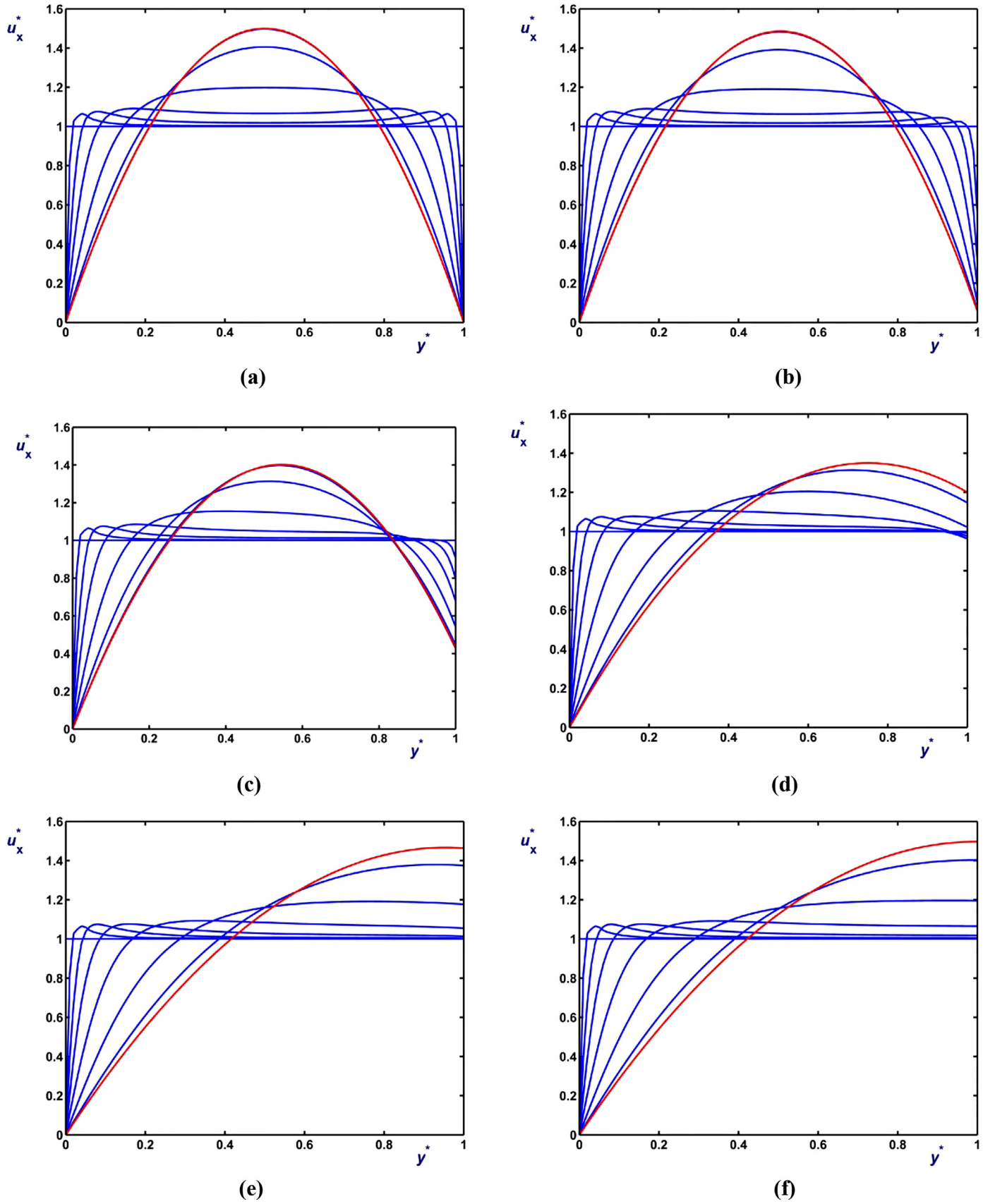

Fig. 6. Development of the velocity in creeping ($Re = 0$) planar Newtonian Poiseuille flow with no-slip along the lower wall and Navier slip ($s = 1$) along the upper one: (a) $B = \infty$ (no-slip); (b) $B = 100$; (c) $B = 10$; (d) $B = 1$; (e) $B = 0.1$; (f) $B = 0.01$. Profiles at $x^* = 0$, 0.02, 0.05, 0.1, 0.2, 0.4, 0.8 and ∞ (fully-developed flow).

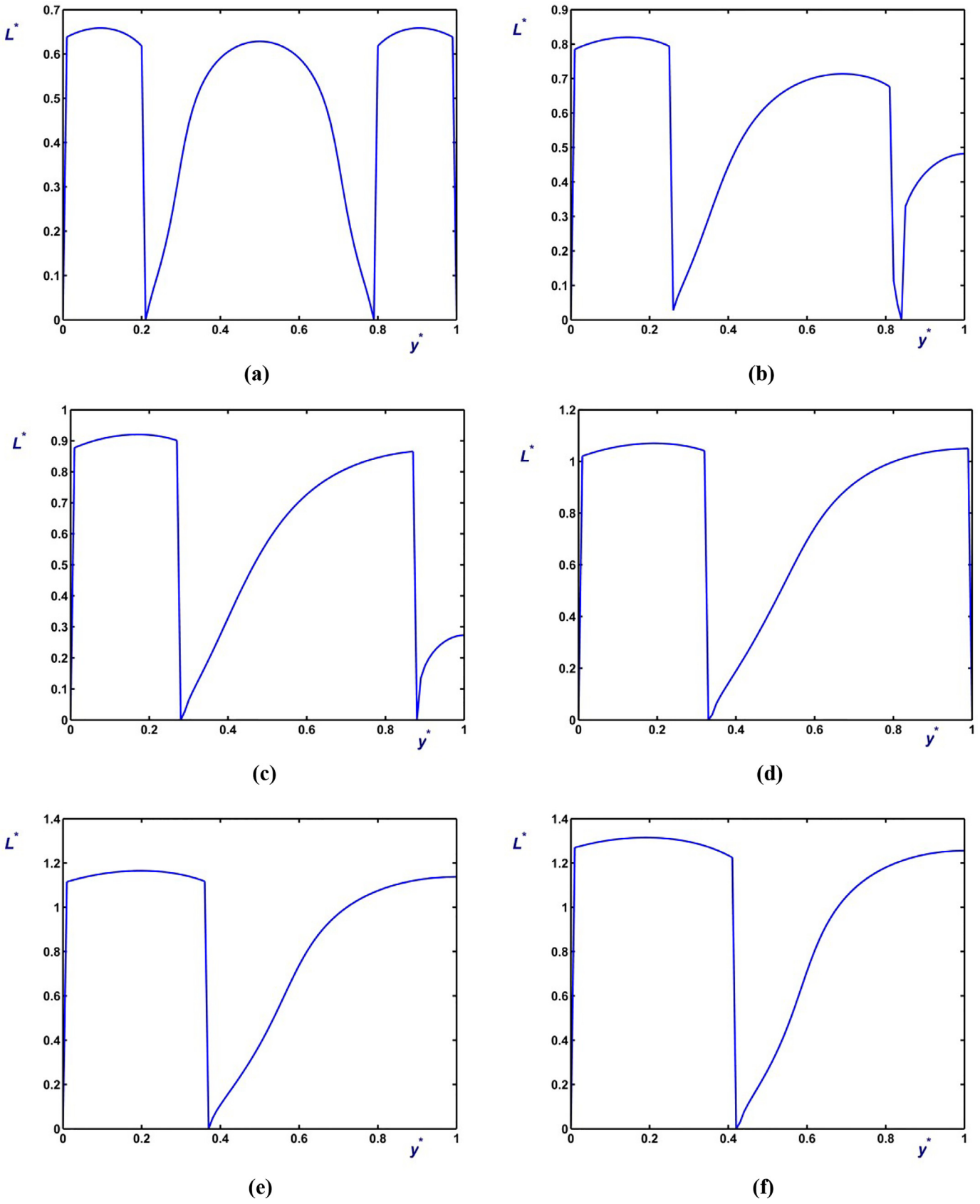

Fig. 7. Development length functions in creeping ($Re = 0$) planar Newtonian Poiseuille flow with no-slip along the lower wall and Navier slip ($s = 1$) along the upper one for the slip numbers of Fig 6:(a) $B = \infty$ (no slip); (b) $B = 10$; (c) $B = 5$; (d) $B = 2$; (e) $B = 1$; (f) $B = 0.01$.

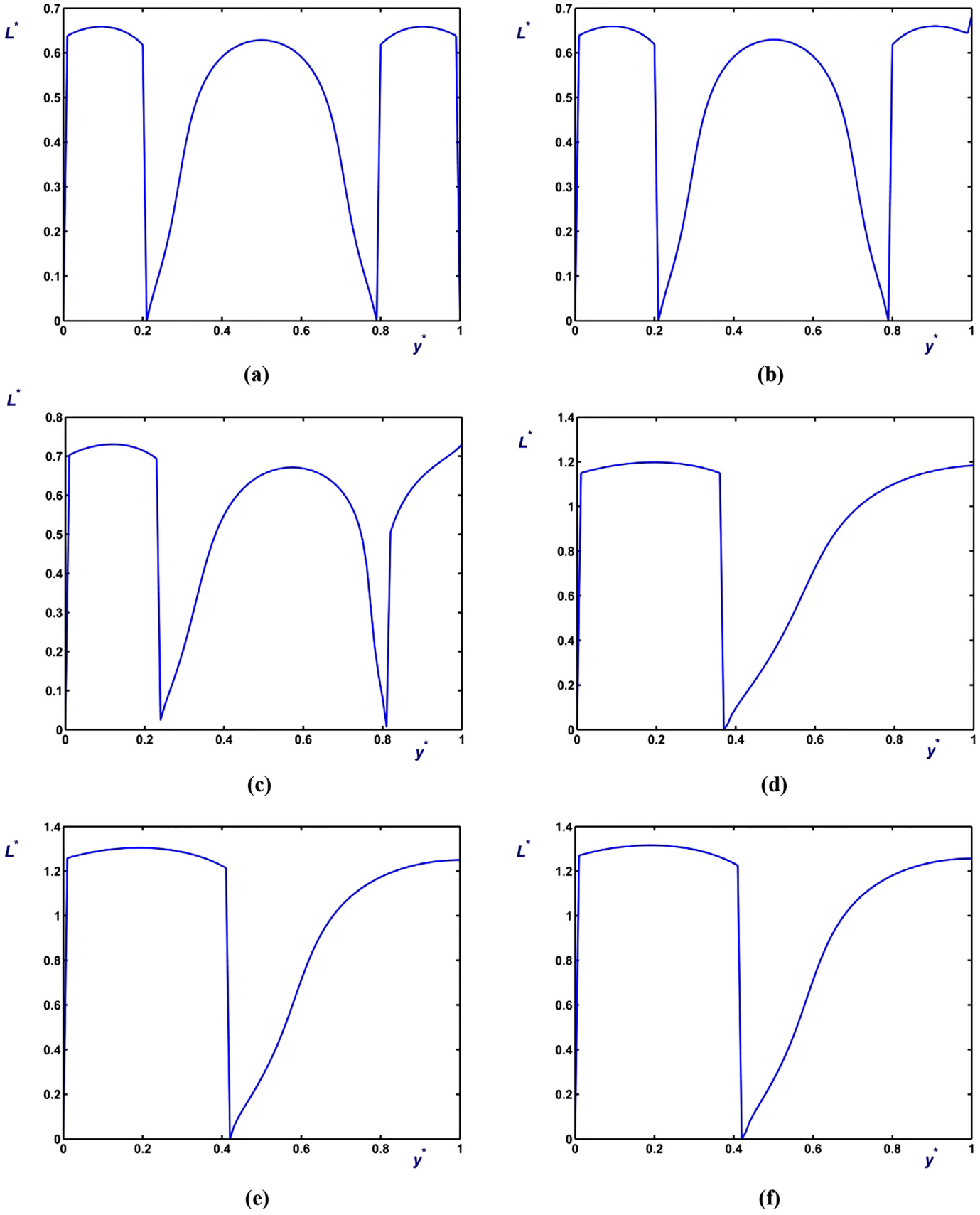

Fig. 8. Development length functions in creeping ($Re = 0$) planar Newtonian Poiseuille flow with no-slip along the lower wall and power-law slip ($s = 1/2$) along the upper one for the slip numbers of Fig 6:(a) $B = \infty$ (no slip); (b) $B = 100$; (c) $B = 10$; (d) $B = 1$; (e) $B = 0.1$; (f) $B = 0.01$.

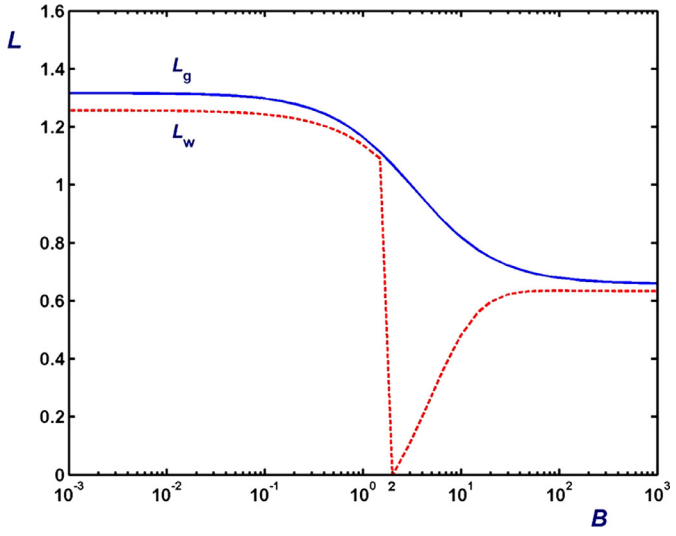

Fig. 9. Global (solid) and wall (dashed) development lengths in creeping ($Re=0$) planar Newtonian Poiseuille flow with no-slip along the lower wall and slip along the upper one versus the slip number B. (a) $s=1$ (Navier slip); (b) $s=1/2$.

2.1.3. Solution in Regime II

If the slip number is reduced below B_c, the yield point keeps moving towards the upper wall and the width of the plug core is thus reduced while its velocity increases. Finally, in the limit $B=0$ (full slip), the velocity profile corresponds to the no-slip solution in a channel of double width ($2H$), i.e. to the no-slip solution corresponding to the modified Bingham number

$$Bn' = \frac{\tau_0 (2H)^n}{kU^n} = 2^n Bn \tag{27}$$

Hence, when $0 < B \le B_c$, the flow corresponds to Regime II and the dimensionless velocity is given by

$$u_x^*(y^*) = \begin{cases} \left[y_1^{*1/n+1} - (y_1^* - y^*)^{1/n+1}\right] \Big/ \left[y_1^{*1/n+1}\left(1 - \dfrac{n}{1+2n} y_1^*\right)\right], & 0 \le y^* \le y_1^* \\ u_w^*, & y_1^* < y^* \le 1 \end{cases} \tag{28}$$

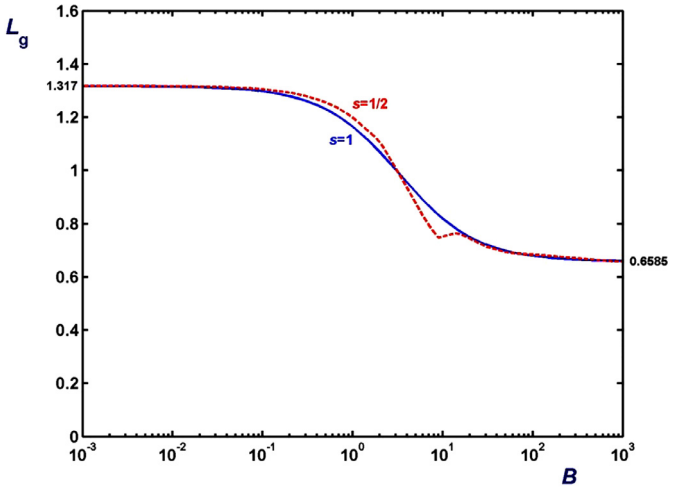

Fig. 10. Global development lengths in creeping ($Re=0$) planar Newtonian Poiseuille flow with no-slip along the lower wall and slip along the upper one with $s=1$ (Navier slip) and $s=1/2$.

where

$$u_w^* = \frac{1}{1 - \frac{n}{1+2n} y_1^*} \tag{29}$$

and y_1^* is the root of

$$(1+1/n)^n (1 - y_1^*) - (Bn + B u_w^{*s}) y_1^{*n+1} / u_w^{*n} = 0 \tag{30}$$

Substituting Eq. (21) into the above equation yields Eq. (25) for y_{1c}^*. For $n=1$ (Bingham plastic) and $s=1$ (Navier slip) Eq. (30) is simplified to

$$Bn\, y_1^{*3} - 3(Bn + B)\, y_1^{*2} - 6 y_1^* + 6 = 0 \tag{31}$$

Before discussing the Herschel–Bulkley solutions, it is instructive to consider the Newtonian case in which the velocity is a parabola. For any value of the slip exponent s, the velocity can be written in the form

$$u_x^* = y^* [6 - 2u_w^* + 3(u_w^* - 2) y^*] \tag{32}$$

where the slip velocity u_w^* is a root of

$$2u_w^* (3 - 2u_w^*) = B u_w^{*s} \tag{33}$$

For example, with $s=1$ (Navier slip)

$$u_w^* = \frac{6}{B+4} \tag{34}$$

and with $s=1/2$

$$u_w^* = \frac{3}{2} - \frac{B^2}{32}\left(\sqrt{1 + \frac{96}{B^2}} - 1\right) \tag{35}$$

When $B=\infty$ (no slip with $u_w^*=0$) and $B=0$ (full slip with $u_w^*=3/2$) the standard no-slip Poiseuille solutions in channels of dimensionless widths 1 and 2, respectively, are recovered, i.e.

$$u_x^* = 6y^*(1 - y^*) \quad \text{and} \quad u_x^* = \frac{3}{2} y^* (2 - y^*)$$

Figs. 3a and b show the velocity profiles for $s=1$ and $s=1/2$, respectively, with $B=\infty$, 10, 1 and 0. It is easily verified that all curves intersect at the point (2/3,4/3), independently of the value of s. Fig. 3c and d show similar velocity profiles for Herschel–Bulkley fluids with $Bn=1$ and $n=1$ (Bingham plastic) and $n=1/2$ in the Navier-slip case ($s=1$). As the slip number is reduced the solution passes from Regime III (two yield points) to Regime II below the critical slip number, which is $B_c=0.7800$ for $n=1$ and 0.8610 for $n=1/2$.

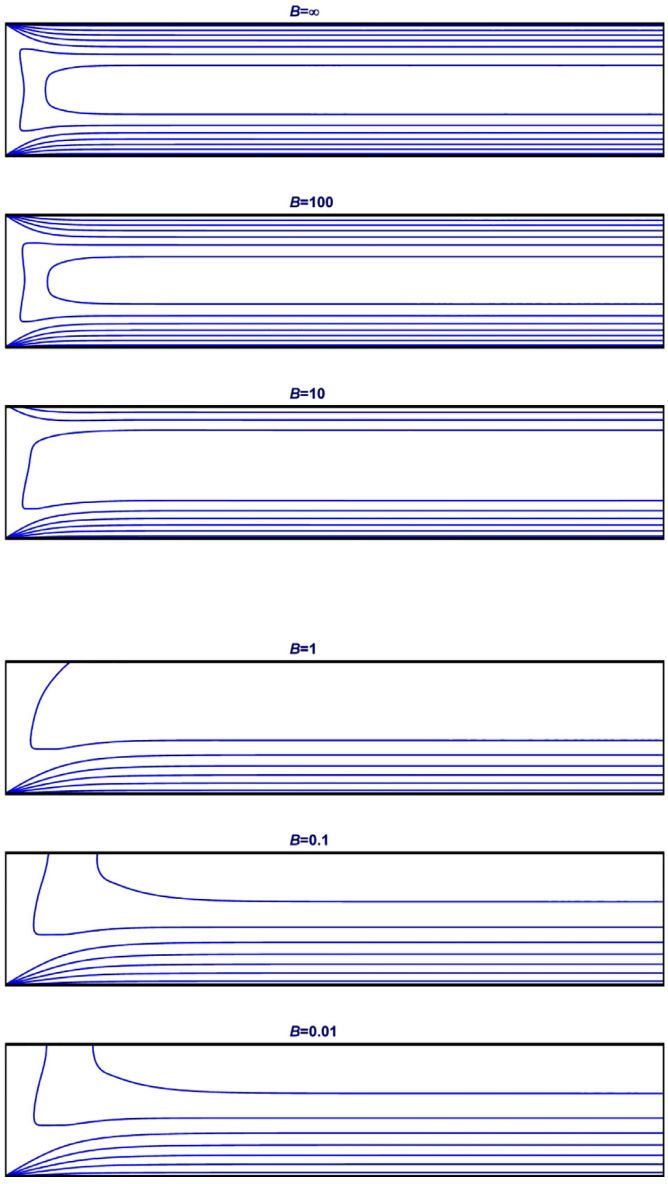

Fig. 11. Velocity contours in flow development of creeping ($Re=0$) planar Bingham-plastic ($n=1$) Poiseuille flow with no-slip along the lower wall and Navier slip ($s=1$) along the upper one for $Bn=1$ and various slip numbers.

Fig. 4 illustrates the two flow regimes on the (Bn,B) plane in the case of a Bingham plastic ($n=1$). These are separated by the curve $B_c=(1-y_{1c}^*/3)Bn$, which is slightly below the straight line $B=Bn$. Four representative velocity profiles, obtained taking $Bn=1$ and Navier slip ($s=1$), are also shown. Two of them are in Regime III. The first profile corresponds to no-slip at both walls ($B\to\infty$) and it is thus symmetric. As slip at the upper wall is enhanced (e.g. for $B=5$), symmetry is destroyed and the two yield points move upwards and the maximum velocity decreases. The upper yield point moves faster than the lower one reaching the wall when $B=B_c=0.7800$. The velocity profile for this critical case is also shown in Fig. 4. Below this number, i.e. in Regime II, the yield point continues moving upwards as slip is increased, but the maximum velocity is now increasing. In the limit of $B=0$ (full slip), the maximum velocity is lower than that for $B\to\infty$, since it corresponds to the no-slip flow for a modified Bingham number equal to $Bn'=2^nBn=2Bn$.

3. Numerical results and discussion

The system of the governing equations and the boundary conditions presented in Section 2 was solved numerically using the finite element method (u-v-p formulation) with standard biquadratic basis functions for the two velocity components and bilinear ones for the pressure field. The Galerkin forms of the continuity and the momentum equations were used. The resulting nonlinear system of the discretized equations was solved with a Newton-Raphson iterative scheme with a convergence tolerance equal to 10^{-4}. The in-house finite-element code developed and tested in the past thirty years (most recently in [17]) was used. Results have been obtained for Bingham numbers ranging from 0 (Newtonian flow) to 10, for power-law exponents from 1 (Bingham plastic) down to 1/2, for slip numbers from 0 (full-slip) to ∞ (no-slip), and for Reynolds numbers from 0 (creeping flow) to 10. Based on our previous studies [17], the rather high value of $M=100{,}000$ has been used in all viscoplastic simulations. For the low Reynolds number considered here, we took $L_{mesh}=20$ for $Re\le 1$ and $L_{mesh}=50$ for $1<Re\le 10$. Some convergence difficulties have been observed in the weak-slip regime (i.e. for finite high values of the slip number B) when the value of n was less than unity. These are due to the fact that the slip velocity is of the order of the convergence tolerance and to the increased nonlinearity of the problem. The convergence of the results has also been investigated using meshes of different refinement. The results presented here have been obtained with a non-uniform mesh consisting of $368\times 80=29{,}440$ elements with 118,657 velocity nodes ($L_{mesh}=20$). The total number of nodal unknowns with this mesh is 267,203. This was graded with the element size increasing far from the walls and the inlet plane. The size of the smallest element at the corner of the inlet plane with the lower wall was 0.005.

3.1. Newtonian flow

The Newtonian flow was investigated first. The effect of Navier slip ($s=1$) on the axial velocity contours in the case of creeping flow ($Re=0$) is illustrated in Fig. 5 for various values of the slip number ranging from $B=\infty$ (no-slip) to $B=0.01$ (very strong slip). When $B=\infty$ the velocity contours are symmetric about the mid-plane of the channel. As slip is introduced at the upper wall the flow becomes more and more asymmetric; in the limit of full slip ($B=0$) the flow corresponds to flow in a channel of double width with no slip at either wall and the upper wall serves simply as the symmetry plane of the latter flow. The flow development for the same slip numbers is also illustrated in Fig. 6, where the velocity profiles at different distances from the inlet are plotted. Note that while the velocity overshoot near the lower wall is unaffected, that near the upper wall appears only when slip is rather weak (i.e. for $B=\infty$ and 100).

In Fig. 7, the plots of the development length function $L(y)$ for all the slip numbers considered in Figs. 5 and 6 are shown. For high values of B there are two decelerating zones adjacent to the walls and one intermediate accelerating zone defined by the two points at which the fully-developed velocity is equal to the mean velocity and thus $L(y)$ vanishes. Below a critical slip number ($\sim$2) slip is so strong that the fluid at the wall actually accelerates and thus the upper deceleration zone disappears. For $B=\infty$ (no-slip at the upper wall), $L(y)$ is of course symmetric. As already pointed out in [17], the global development length L_g does not occur in the accelerating zone at the plane of symmetry but in the two symmetric decelerating zones near the walls ($L_g=0.6585$, whereas the classical center-plane development length is $L_c=0.6285$). In the no-slip case the upper-wall development length, defined by $L_w\equiv L(1)$, is not relevant. As slip along the upper wall is enhanced so does the asymmetry and the flow develops faster near the upper wall

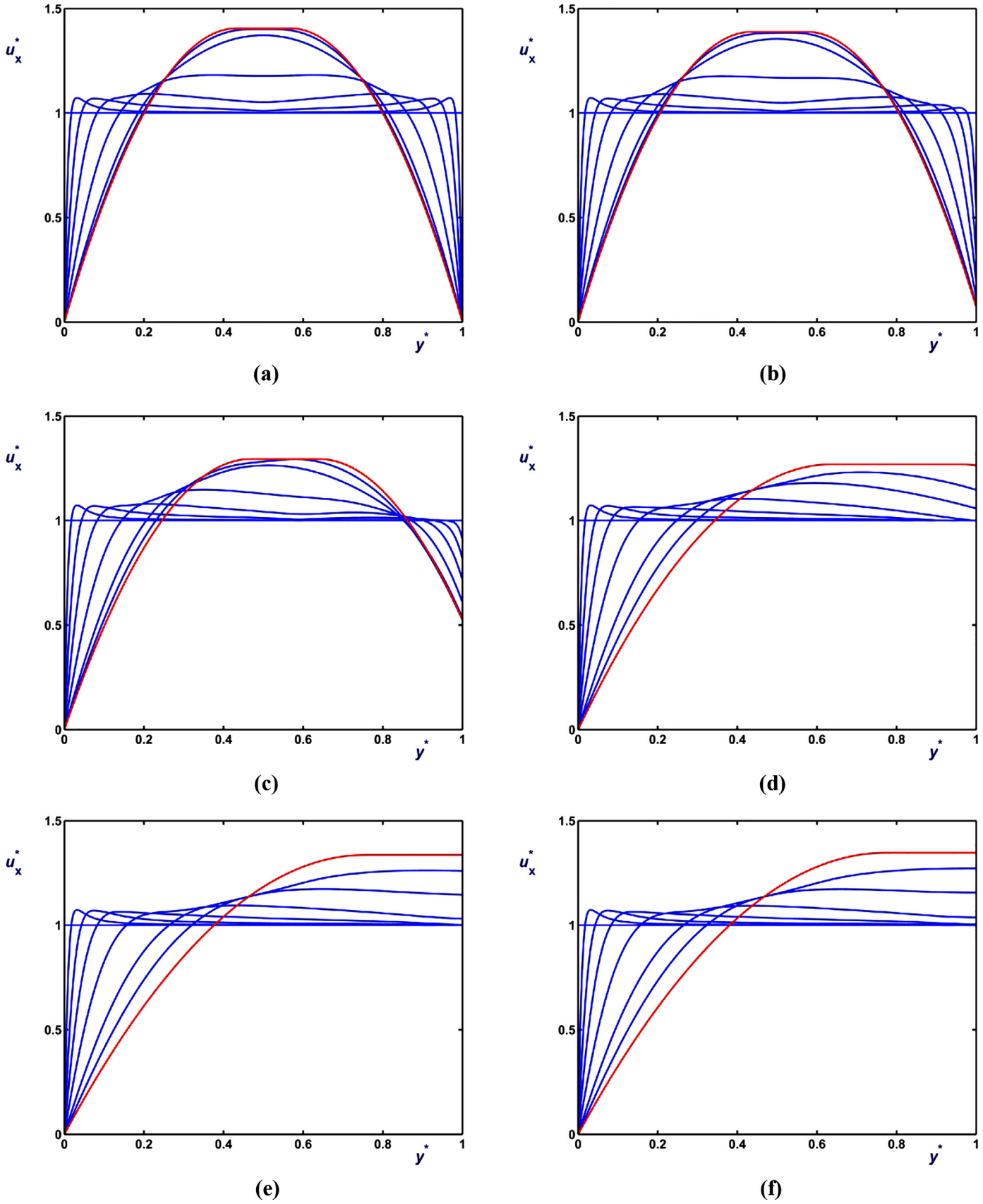

Fig. 12. Development of the velocity in creeping ($Re = 0$) planar Bingham-plastic ($n = 1$) Poiseuille flow with no-slip along the lower wall and Navier slip ($s = 1$) along the upper one with $Bn = 1$: (a) $B = \infty$ (no-slip); (b) $B = 100$; (c) $B = 10$; (d) $B = 1$; (e) $B = 0.1$; (f) $B = 0.01$. Profiles at $x^* = 0$, 0.02, 0.05, 0.1, 0.2, 0.4, 0.6 and ∞ (fully-developed flow).

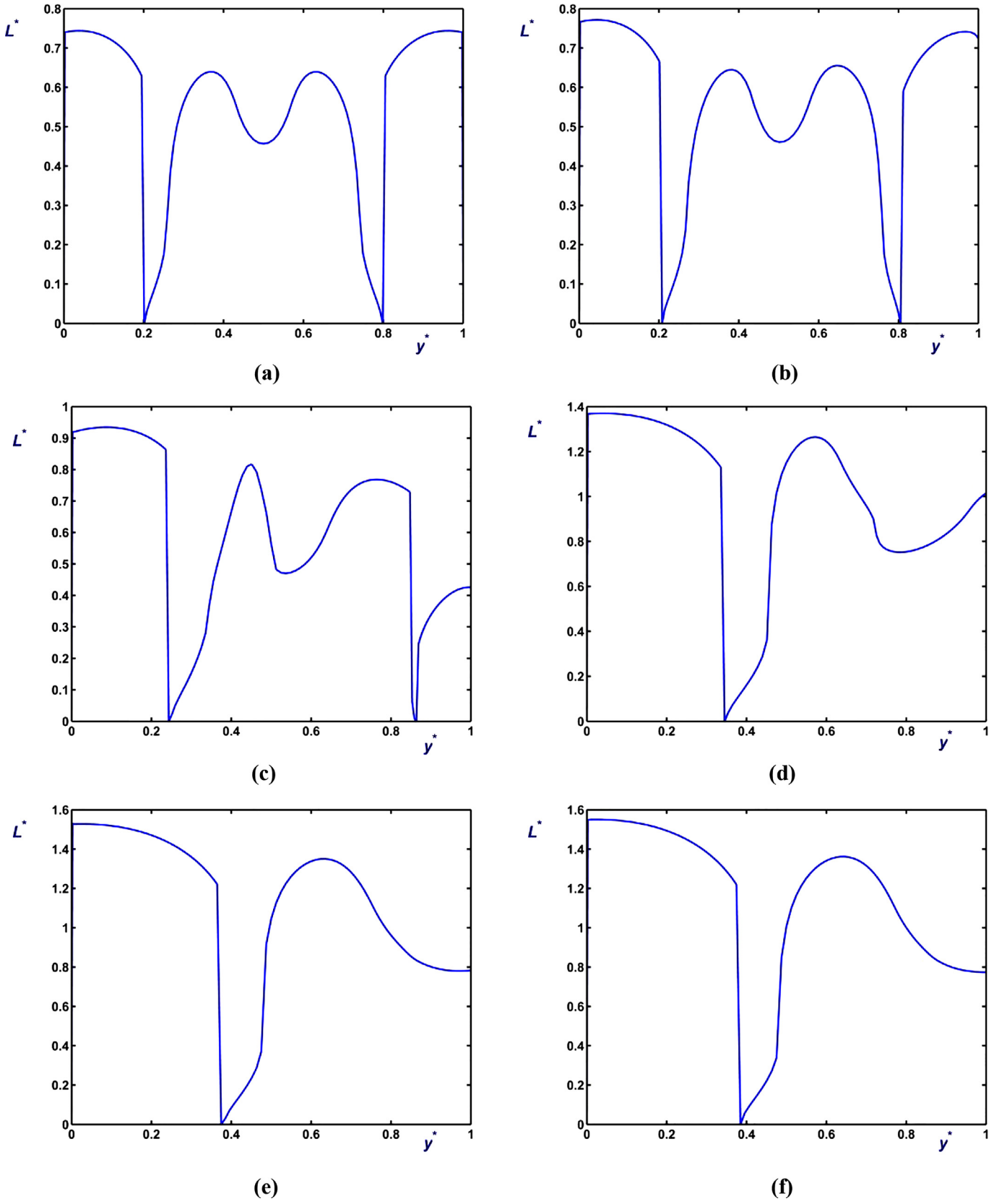

Fig. 13. Development length functions in creeping ($Re = 0$) planar Bingham-plastic ($n = 1$) Poiseuille flow with no-slip along the lower wall and Navier slip ($s = 1$) along the upper one for $Bn = 1$ and the slip numbers of Fig 10: (a) $B = \infty$ (no slip); (b) $B = 100$; (c) $B = 10$; (d) $B = 1$; (e) $B = 0.1$; (f) $B = 0.01$.

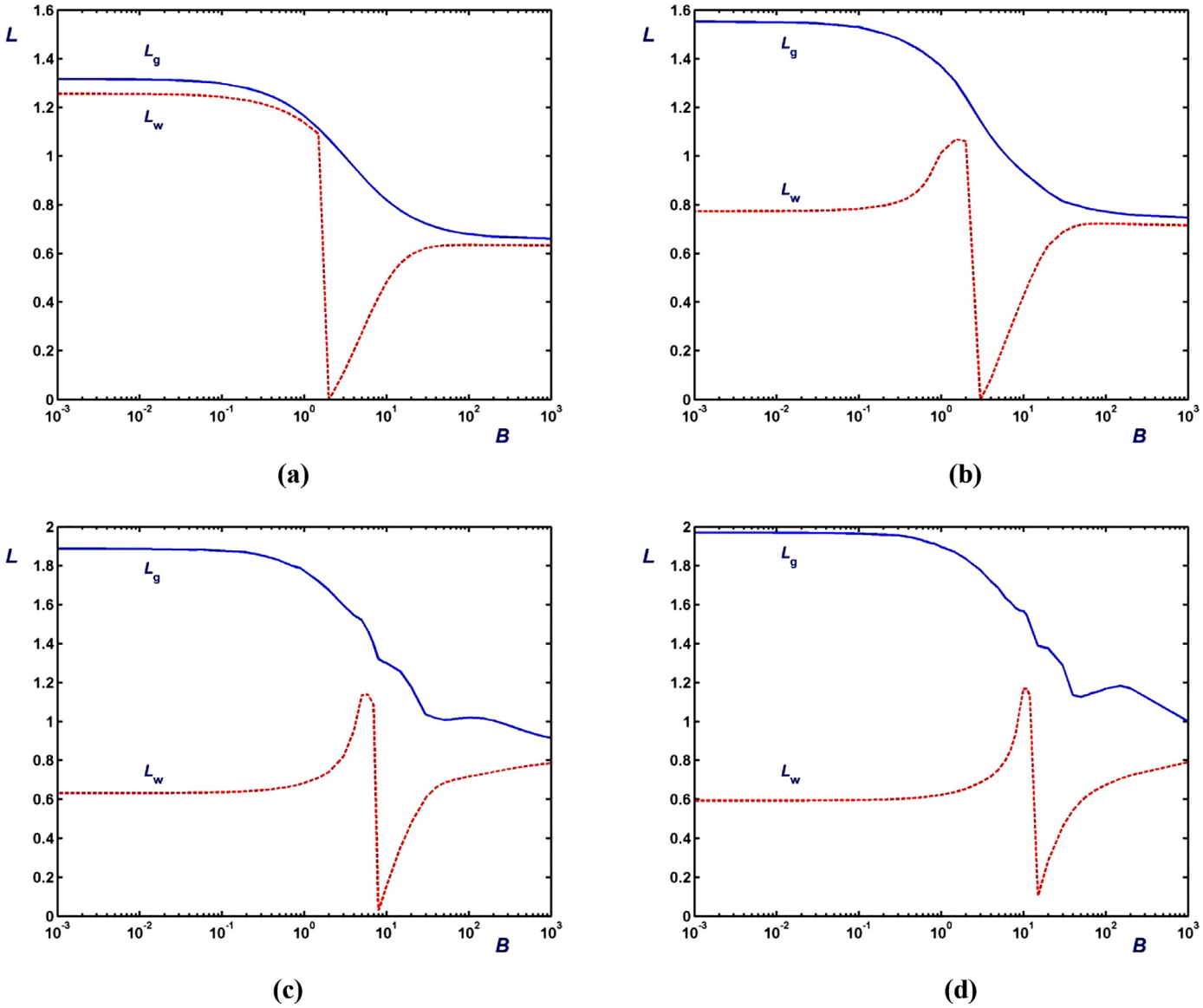

Fig. 14. Global (solid) and wall (dashed) development lengths in creeping ($Re = 0$) planar Bingham-plastic Poiseuille flow with no-slip along the lower wall and Navier slip ($s = 1$) along the upper one versus the slip number B: (a) $Bn = 0$ (Newtonian); (b) $Bn = 1$; (c) $Bn = 5$; (d) $Bn = 10$.

where slip occurs and near the lower wall more slowly so that the global development length increases (note that the y-axis is not the same). Hence, L_g occurs in the lower decelerating zone and L_w is much less than L_g. As B is reduced, L_g keeps increasing, while L_w is further reduced till the upper decelerating zone disappears, in which case the fluid at the upper wall actually accelerates and consequently there is only one decelerating region near the lower wall. Thus, below a certain slip number both L_g and L_w increase as B is reduced. The global development length increases asymptotically to twice its counterpart for the no-slip flow, i.e. $L_g = 1.3168$.

In order to investigate the effect of the slip exponent s, calculations similar to those of Figs. 5–7 have been carried out taking $s = 1/2$. It turns out that the velocity contours are not affected significantly, but, given that the fully-developed slip velocities for $s = 1/2$ are lower, there are some noticeable differences between the velocity profiles, especially when slip is weak, i.e. for high or moderate values of the slip number. Interestingly, the slip exponent has a striking effect on the development length. (It should be noted that the dimensionless slip number depends on s.) As shown in Fig. 8, with $s = 1/2$ the flow development for high values of B (weak slip) is slower in the zone near the upper wall rather than in the zone near the lower (no-slip) wall.

The dependence of the two development lengths on the slip number B for $s = 1$ and $1/2$ is illustrated in Fig. 9. L_g increases with slip exhibiting two plateaus in the weak- and strong-slip limits and a sharp change in the range (0.5, 5) of the slip number. The wall development length L_w exhibits a sharp non-monotonic behavior in the latter range due to the suppression and the disappearance of the decelerating region near the upper wall and vanishes at the critical slip number $B = 2$ at which $u_w^* = 1$, independently of the slip exponent s (see Eq. (33)). With $s = 1$, L_w is always less than L_g, while with $s = 1/2$ the two lengths coincide when slip is weak. As pointed out in Ref. [16], the wall development length can be defined only if the magnitude of the slip velocity exceeds a critical value. By demanding that 1% of the critical slip velocity must be equal to the tolerance used in the numerical simulations, then this critical slip velocity is equal to 0.01. From Eq. (33), the corresponding critical value of the slip number is then $B_{crit} = 5.96 \times 10^{2s}$. We thus find that $B_{crit} = 596$ for $s = 1$ and $B_{crit} = 59.6$ for $s = 1/2$. Therefore, the plots of L_w beyond these crit-

ical values in Fig. 9 (i.e. in the weak-slip regime) should be viewed with caution. Note also that the wiggle in the curve of L_g is simply due to the fact as slip is increased the flow development is initially slower in the upper deceleration zone which eventually disappears and thus the value of L_g is suddenly calculated in the lower deceleration zone. The global development lengths for $s=1$ and $s=1/2$ are compared in Fig. 10. As expected, the two lengths differ only for moderate values of the slip number and practically coincide in both the weak- and strong-slip regimes, where the effect of the slip exponent is insignificant. It should be noted that the development length corresponding to full slip ($B=0$) is twice the development length for the no-slip case (infinite B), since it corresponds to the no-slip flow in a channel of a gap width equal to 2.

3.2. Viscoplastic flow

In this subsection, numerical results for Bingham plastics ($n=1$) and Herschel–Bulkley fluids ($n=1/2$) are discussed. We then considered the Bingham plastic case ($n=1$) with $Bn=1$ for $Re=0$ (creeping flow). Fig. 11 shows the axial velocity contours for various values of the slip number B. Fig. 12 shows how the velocity component in the flow direction develops downstream attaining the fully developed profile. When $B=\infty$ (no slip), the velocity profiles are symmetric exhibiting a central unyielded region. As slip is increased, asymmetry is enhanced, the velocity overshoot near the upper wall is suppressed, and the unyielded region moves towards the upper wall and increases in size. If slip becomes even stronger then Regime II is eventually reached, i.e. the unyielded region reaches the upper wall. The velocity overshoot near the no-slip wall persists in all cases, while its counterpart near the slip wall appears only when slip is weak (i.e. for high values of B).

The development length functions for various values of the slip number are shown in Fig. 13. These plots may be more complicated than their Newtonian counterparts in Fig. 8 but the main features remain the same: (a) L_g occurs near the no-slip wall, i.e. the flow develops more slowly in the decelerating zone adjacent to the no-slip wall than in the accelerating zone; (b) The fluid adjacent to the upper wall decelerates only when slip is weak, i.e. above a critical slip number.

Similar results have been obtained for higher values of the Bingham number. In Fig. 14, the global and wall development lengths for creeping flow ($Re=0$) and $Bn=0$ (Newtonian), 1, 5 and 10 are plotted versus the slip number. We observe that L_g increases with slip and with the Bingham number, whereas L_w exhibits a non-monotonic behavior. When slip is strong, L_w decreases rapidly with Bn. For moderate slip numbers, however, the dependence of L_w on the Bingham number is variable. It is clear that using L_w may lead to erroneous results regarding flow development. The global development lengths for $Bn=0$, 1, 5, and 10 are compared in Fig. 15. Based on L_g, flow development is slower as viscoplasticity and slip are increased. Again, the wiggles in the curves for $Bn=5$ and 10 indicate transition of L_g to a different deceleration or acceleration zone. As mentioned above, in Newtonian flow ($Bn=0$) the development length for full slip ($B=0$) is two times the development length for the no-slip case (infinite B), since it corresponds to the flow development in a channel with no slip and with a gap width equal to 2. This is not the case for Bingham flow; the development length in the full-slip case is two times the no-slip development length corresponding to $2Bn$ and not to Bn.

Simulations have also been carried out for Herschel–Bulkley flow with $Bn=1$, $n=1/2$ and $s=1$ (Navier slip). The global development lengths for $n=1$ and $n=1/2$ are compared in Fig. 16. As expected, shear thinning results in bigger development lengths. Finally, the effect of the Reynolds number is illustrated in Fig. 17, where the global development length for $Bn=1$ and $Re=0$, 1, and 10 is plotted versus the slip number. For the moderate numbers

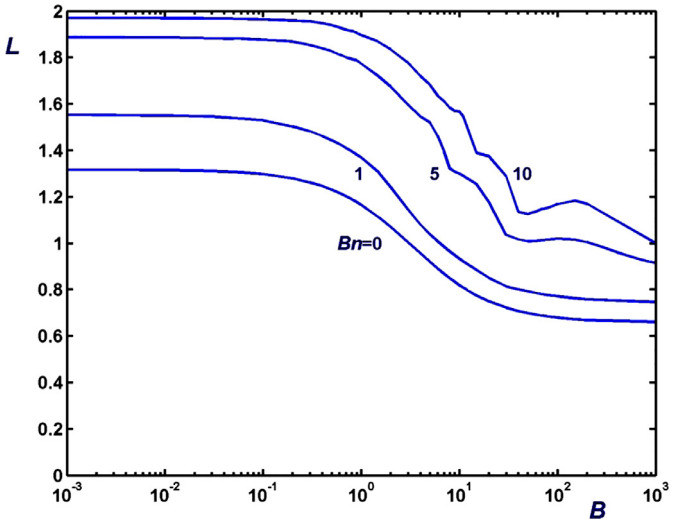

Fig. 15. Global development lengths in creeping ($Re=0$) planar Bingham-plastic Poiseuille flow with no-slip along the lower wall and Navier slip ($s=1$) along the upper one versus the slip number B for different Bingham numbers.

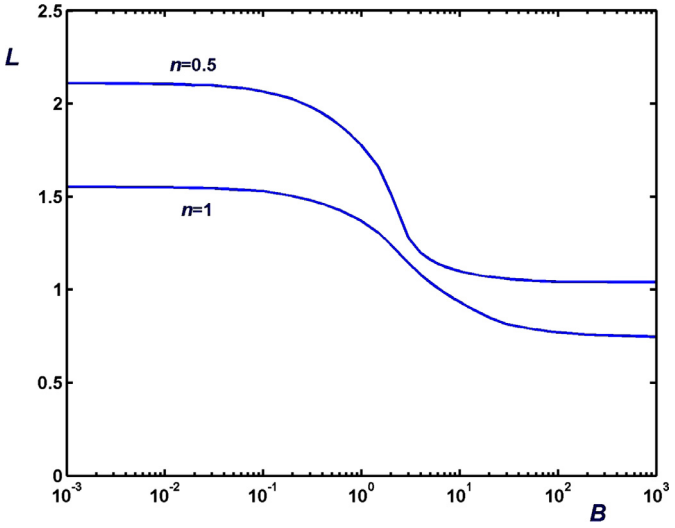

Fig. 16. Global development lengths in creeping ($Re=0$) planar Herschel–Bulkley Poiseuille flow with no-slip along the lower wall and Navier slip ($s=1$) along the upper one versus the slip number B for $Bn=1$ and $n=1$ (Bingham plastic) and $n=1/2$.

employed here, the global development length increases with inertia. The relative increase of L_g is much higher when slip is weak, moderate in the strong-slip regime, and becomes smaller in the intermediate slip regime when the upper deceleration zone disappears.

An interesting issue not addressed in the present work is the accurate determination of yielded and unyielded regions in viscoplastic flow development. Our calculations with "reasonable" meshes showed that this may not be possible for moderate or higher Bingham numbers. More acceptable results, in the sense that the entry unyielded region which moves horizontally as a solid body at unit velocity is separated from the unyielded region of the fully-developed flow which moves at a higher velocity, may be obtained for rather low Bingham numbers. At higher Bingham numbers these two regions appear to merge, which is obviously inadmissible. Hence, the flow development problem is a challenging test for any numerical method proposed for solving viscoplastic flows. To our knowledge, only recently Dimakopoulos

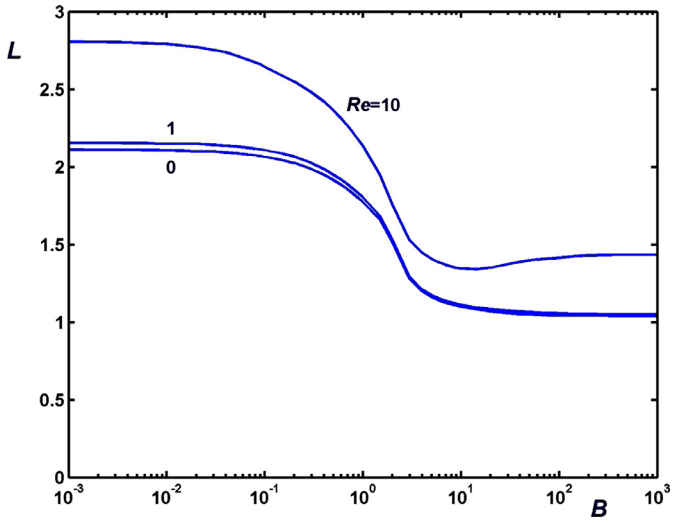

Fig. 17. Global development lengths in planar Herschel–Bulkley Poiseuille flow with no-slip along the lower wall and Navier slip ($s=1$) along the upper one versus the slip number B for different Reynolds numbers, $Bn=1$ and $n=1/2$.

et al. [19] made some preliminary calculations of yielded/unyielded regions in viscoplastic flow development and compared the predictions of the Augmented Lagrangian Method (ALM) and the regularization method.

4. Conclusions

The entry flow of a Herschel–Bulkley fluid in a horizontal channel with slip along the upper wall has been investigated numerically using finite elements and the Papanastasiou regularization for the constitutive equation. The different flow regimes for the one-dimensional fully-developed flow were identified and the corresponding solutions have been presented. The global development length is considered so that both the acceleration and deceleration zones are included. Representative numerical solutions for the two-dimensional flow development have been presented and the effects of the Bingham and slip numbers on the development of the velocity and on the development length have been discussed for various values of the power-law exponent of the slip equation. The global development length increases with the Bingham number and inertia and decreases with the power-law exponent. In general, the global development length increases with slip exhibiting two plateaus for low and strong slip and a sharp increase in the moderate slip regime.

References

[1] E. Mitsoulis, Flows of viscoplastic materials; models and computation, Rheol. Rev. 2007 (2007) 135–178.
[2] N.J. Balmforth, I.A. Frigaard, G. Ovarlez, Yielding to stress: recent developments in viscoplastic fluid mechanics, Annu. Rev. Fluid Mech. 46 (2014) 121–146.
[3] T.C. Papanastasiou, Flows of materials with yield, J. Rheol. 31 (1987) 385–404.
[4] K.R.J. Ellwood, G.C. Georgiou, T.C. Papanastasiou, J.O. Wilkes, Laminar jets of Bingham plastic liquids, J. Rheol. 34 (1990) 787–812.
[5] E. Mitsoulis, J. Tsamopoulos, Numerical simulations of complex yield-stress fluid flows, Rheol. Acta 56 (2017) 231–258.
[6] P. Saramito, A. Wachs, Progress in numerical simulation of yield stress fluid flows, Rheol. Acta 56 (2017) 211–230.
[7] U. Yilmazer, D.M. Kalyon, Slip effects in capillary and parallel disk torsional flows of highly filled suspensions, J. Rheol. 33 (1989) 1197–1212.
[8] P. Ballesta, G. Petekidis, L. Isa, W.C.K. Poon, R. Besseling, Wall slip and flow of concentrated hard-sphere colloidal suspensions, J. Rheol. 56 (2012) 1005–1037.
[9] M. Cloitre, R.T. Bonnecaze, A review on wall slip in high solid dispersions, Rheol. Acta 56 (2017) 283–305.
[10] M.M. Denn, Extrusion instabilities and wall slip, Annu. Rev. Fluid Mech. 33 (2001) 265–287.
[11] D.M. Kalyon, Apparent slip and viscoplasticity of concentrated suspensions, J. Rheol. 49 (2005) 621–640.
[12] C.L.M.H. Navier, Sur les lois du mouvement des fluides, in: Mémoires de l'Academie des Sciences de l'Institute de France, 6, 1827, pp. 389–440.
[13] A.L. Vayssade, C. Lee, E. Terriac, F. Monti, M. Cloitre, P. Tabeling, Dynamical role of slip heterogeneities in confined flows, Phys. Rev. 89 (2014) 052309.
[14] P. Panaseti, G.C. Georgiou, A.L. Vayssade, M. Cloitre, Confined viscoplastic flows with heterogeneous wall slip, Rheol. Acta 56 (2017) 539–553.
[15] R. Shah, A. London, Laminar Flow Forced Convection in Ducts: A Source Book for Compact Heat Exchanger Analytical Data, Academic Press, 1978.
[16] Z. Kountouriotis, M. Philippou, G.C. Georgiou, Development lengths in Newtonian Poiseuille flows with wall slip, Appl. Maths. Comp. 291 (2016) 98–114.
[17] M. Philippou, Z. Kountouriotis, G.C. Georgiou, Viscoplastic flow development in tubes and channels with wall slip, J. Non-Newtonian Fluid Mech. 234 (2016) 69–81.
[18] S. Ookawara, K. Ogawa, N. Dombrowski, E. Amooie-Foumeny, A. Riza, Unified entry length correlation for Newtonian, power law and Bingham fluids in laminar pipe flow at low Reynolds numbers, J. Chem. Eng. Jpn. 33 (2000) 675–678.
[19] Y. Dimakopoulos, G. Makrygiorgos, G.C. Georgiou, J. Tsamopoulos, A fast and efficient algorithm for computing viscoplastic flows, 8th International Meeting of the Hellenic Society of Rheology, Limassol, Cyprus, July 12–14, 2017.